CrossMark
click for updates

Enhanced visible light response of a WO₃ photoelectrode with an immobilized fibrous gold nanoparticle assembly using an amyloid-β peptide†

Akira Onoda,*[a] Hirofumi Harada,[a] Taro Uematsu,[ab] Susumu Kuwabata,[a]
Ryo Yamanaka,[c] Shinichi Sakurai[c] and Takashi Hayashi*[a]

A WO₃ photoelectrode immobilizing a fibrous gold nanoparticle (AuNP) assembly using an amyloid-β (Aβ) peptide was constructed and its ability for photocurrent generation upon visible light irradiation was investigated. AuNPs attached using Aβ peptide (Aβ-AuNP) assemble with a fibrous structure at pH 4.5, which disperses at pH 11. The modified Aβ-AuNPs are immobilized on the surface of WO₃ fabricated on a fluorine-doped tin oxide (FTO) electrode (Aβ-AuNP$_{ass}$@WO₃/FTO or Aβ-AuNP$_{dis}$@WO₃/FTO, respectively). The photocurrent generation response of the Aβ-AuNP$_{ass}$@WO₃/FTO electrode is clearly increased relative to that of Aβ-AuNP$_{dis}$@WO₃/FTO upon visible light irradiation (λ = 420–750 nm), indicating that the fibrous AuNP assembly enhances the visible light response of the WO₃ photoelectrode.

Metal nanoparticle–semiconductor (MNP–SC) composites have emerged as a novel class of photocatalysts for a wide range of chemical reactions and photoelectrochemical conversions.[1–8] Although a variety of semiconductor photocatalysts are known to function under UV light, strategies for improving the visible light response of photocatalysts are required for the efficient use of solar energy. WO₃ is an attractive n-type semiconductor photocatalyst providing a positive conduction band edge lower than the water oxidation potential. However, the band gap energy of WO₃ (∼2.6 eV) is sufficiently large to absorb visible light. To improve the visible light response, we investigate a WO₃ photocatalyst capable of immobilizing noble metal nanoparticles that have strong surface plasmon resonance (SPR).[9–13]

An interfacial structure between semiconductor and nanoparticles in hybrid composites has been identified as crucial feature that improves reactivities and photochemical properties of MNP–SCs.[14–16] The properties of immobilized MNPs including SPR absorption, refractive index, and light scattering, which are affected by MNP composition, size, and shape, are important parameters to explore in development of new features in MNP–SC materials. We have therefore focused on developing a method to immobilize MNP assemblies on the surface of SCs. Recently, we reported a TiO₂ composite which immobilizes AuNP assemblies *via* the biotin–streptavidin interaction. This enables efficient electron transfer from TiO₂ to immobilized AuNPs as indicated by photocatalytic activity.[17] An amyloid-β (Aβ) peptide, which accumulates as the major constituent of the extracellular deposits in Alzheimer's disease, forms fibrous aggregates.[18] It is known that the Aβ peptide is useful in assembling the metal nanoparticles when linked to the surface of the metal,[19,20] thereby the Aβ peptide is advantageous to provide tight interaction between AuNPs. Here, we report a new method for preparing AuNP–WO₃ composites with fibrous AuNP assemblies using amyloid formation promoted by the Aβ peptide (Fig. 1). The unique AuNP assembly on the WO₃ surface further improves the photocurrent generation upon visible light irradiation.

The soluble Aβ peptide fragment (consisting of residues 1–16 of amyloid-β)[19] whose aggregation depends on pH was linked to a GGGC fragment at the C-terminus for immobilization on the AuNP surface. This component was synthesized by standard solid-phase peptide synthesis. The crude peptide was purified by HPLC and characterized by ESI-TOF MS (Fig. S1, ESI†). The folding and assembling properties of the Aβ peptide with the additional fragment were investigated by obtaining CD measurements (Fig. S2, ESI†). The Aβ peptide exhibits a strong negative minimum at 205 nm both at pH 11 and 7, suggesting prevalent random coil structure. In contrast, Aβ has a positive maximum at 220 nm in a buffer adjusted to pH 4.5. This feature is consistent with the reported result.[19] The result indicates that the modified Aβ peptide retains the inherent ability to assemble as β-sheet.

[a]*Department of Applied Chemistry, Graduate School of Engineering, Osaka University, Suita, 565-0871, Japan. E-mail: onoda@chem.eng.osaka-u.ac.jp; thayashi@chem.eng.osaka-u.ac.jp*

[b]*Frontier Research Base for Global Young Researchers, Graduate School of Engineering, Osaka University, Suita, 565-0871, Japan*

[c]*Department of Biobased Materials Science, Kyoto Institute of Technology, Matsugasaki, Sakyo-ku, 606-8585, Japan*

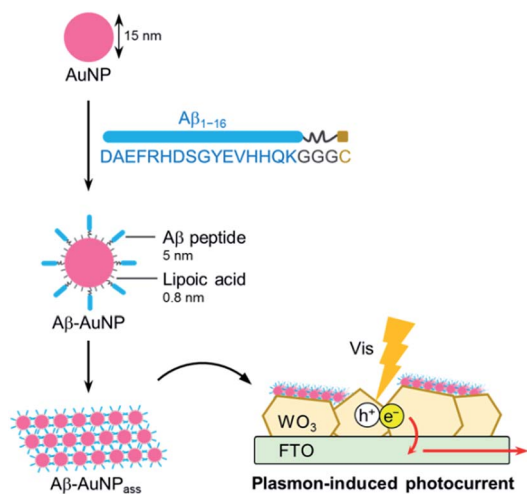**Fig. 1** Preparation of a WO₃ composite with fibrous AuNP assembly using amyloid-β.

The Aβ peptide was immobilized on the surface of the gold nanoparticle through an Au–S bond with the C-terminal Cys residue. AuNP modified with a lipoic acid was treated with the Aβ peptide. The mixed solution of AuNP and the Aβ peptide was incubated for 24 h at 25 °C. Immobilization of the peptide *via* a Cys moiety on the AuNP surface was confirmed by agarose gel electrophoresis (Fig. 2a). The negatively-charged AuNP covered with lipoic acid runs smoothly towards the anode. Interestingly, Aβ-AuNP has clearly shifted bands due to its increased size and

decreased negative charge (Fig. 2a). In addition, titration experiments with gel electrophoresis indicate that approximately 300 strands of the Aβ peptide are connected to each AuNP particle. This result clearly shows that the Aβ peptides modify the surface of the AuNP particle *via* the Cys residue.

The assembly properties of Aβ-AuNP were analyzed by SPR absorption at different pH values including pH 11, 7, and 4.5 (Fig. 2b). The SPR peak of the AuNP was observed at 523 nm at pH 11 and 7. The red color of Aβ-AuNP changes to purple at pH 4.5 and an intense absorption peak arises at 675 nm. The red-shifted absorption indicates that AuNPs are assembled and that the average of the interparticle distance is shorter under acidic condition. The assembled structure of Aβ-AuNP was analyzed by atomic force microscopy (AFM) (Fig. 2c–e). The sample solution was drop-casted on a glass surface for the measurement. When we observed Aβ-AuNP at pH 11 and 7, the AuNPs were found to be uniformly connected and immobilized on the surface. In contrast, we found that the Aβ-AuNPs are assembled as a fibrous structure at pH 4.5. The AuNP tightly assembled as a nanofiber provides a significantly shifted SPR absorption.

The assembling feature of Aβ-AuNP was further analyzed by small angle X-ray scattering (SAXS) (Fig. 3). AuNPs modified only with lipoic acid (LA-AuNP) are compared as a reference (Fig. S3†). Interestingly, the SAXS profiles obtained from the dropcast sample on a polyimide film show peaks in a low q region ($q < 0.5$ nm^{-1}), which was not found in the profiles in solution. These new peaks indicate the formation of the AuNP assembly. The d-spacing of Aβ-AuNP (17.2 nm at pH 11, 16.1 nm
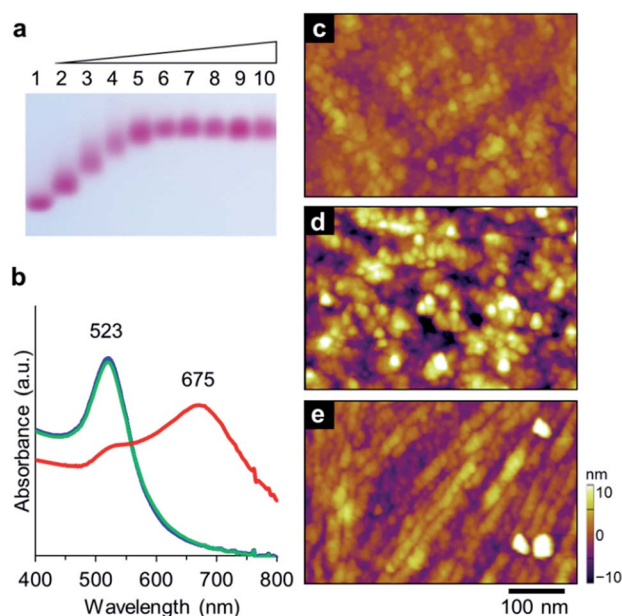

Fig. 2 (a) Agarose gel electrophoresis of Aβ-modified AuNPs. The concentration of Aβ increases from lane 1 to 10 (0, 80, 160, 240, 320, 390, 470, 550, 630, and 710 eq.) *vs.* AuNP (per particle). (b) UV/vis absorption spectra of Aβ-AuNP at pH 11 (blue), pH 7.0 (green), and pH 4.5 (red) in 10 mM KPi or NaOAc buffer. AFM images of Aβ-AuNP at (c) pH 11, (d) pH 7.0, and (e) pH 4.5. The sample solution at an adjusted pH was casted onto a glass plate.
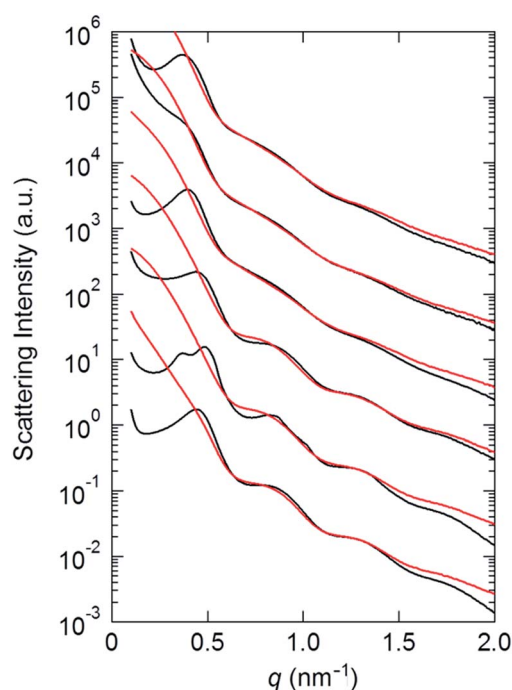

Fig. 3 SAXS profiles plotted as scattering intensity ($I(q)$) *vs.* magnitude of scattering vector (q). The SAXS profile of the sample in cast film (black line) and in solution (red). From top; the profiles of Aβ-AuNP at pH 11, 7, 4.5, and LA-AuNP without Aβ peptide at pH 11, 7, 4.5.

at pH 7 and pH 4.5) increases relative to the values in LA-AuNP (14.3 nm at pH 11, 16.1 and 15.9 nm at pH 7, 14.3 nm in pH 4.5). This result suggests that the modification of the AuNP with the Aβ peptide provides a unique assembly mode. In addition, the observed d value of 17.2 nm for Aβ-AuNP at pH 11 decreases to 15.9 nm at pH 4.5. This appears to correspond with the fibrous morphology that we observed in AFM imaging.

The AuNP assembly using the Aβ peptide was immobilized on WO_3 fabricated on fluorine doped tin oxide (FTO) electrode. The crystal of WO_3 was grinded in a solution of 0.5% diacetyl cellulose using a ball mill. The resulting solution of WO_3 was drop-casted onto the FTO electrode and the electrode was heated to 450 °C and incubated for 2 h. The WO_3/FTO electrode was then immersed in the solution of Aβ-AuNP at pH 4.5 or pH 11 to immobilize AuNPs, and the two electrodes, Aβ-AuNP$_{ass}$@WO_3/FTO and Aβ-AuNP$_{dis}$@WO_3/FTO, were prepared. The electrode immobilizing AuNP without the Aβ peptide was also prepared (LA-AuNP@WO_3/FTO). SEM analysis indicates that the AuNPs with the size of $ca.$ 15 nm are immobilized on the surface of Aβ-AuNP$_{ass}$@WO_3/FTO (Fig. 4a and b). The elemental mapping by EDX also supports the existence of Au and S atoms of AuNPs on the surface (Fig. S4, ESI†). The AuNP assembly was observed in large area of the WO_3 surface in Aβ-AuNP$_{ass}$@WO_3/FTO. A similar large area of AuNP was not found in Aβ-AuNP$_{dis}$@WO_3/FTO or LA-AuNP@WO_3/FTO immobilizing AuNP without the Aβ peptide (Fig. S5, ESI†).

Immobilization of Aβ-AuNP on the surface of the WO_3/FTO electrode was confirmed by diffuse reflection spectra (Fig. 4c). WO_3 absorbs UV-light ($λ < 400$ nm), and, Aβ-AuNP$_{dis}$@WO_3/FTO has SPR absorption at 523 nm. In contrast, the WO_3 electrode

immobilizing the Aβ-AuNP assembly (Aβ-AuNP$_{ass}$@WO_3/FTO) has the peak maxima shifted to 590 and 680 nm. The SPR redshift is consistent with that observed in solution, suggesting that the Aβ-AuNP forms a fibrous assembly as visualized in AFM experiments.

Photocurrent measurements of Aβ-AuNP$_{ass}$@WO_3/FTO and Aβ-AuNP$_{dis}$@WO_3/FTO electrodes were performed to investigate sensitization of fibril-like assemblies of AuNP. Photocurrent response patterns of the AuNP-immobilized electrodes were measured during on/off cycles of visible light (420–750 nm) in the presence of 2-propanol as an electron donor (Fig. 5a). We observed clear rise and fall of the anodic current under the bias potential of +0.3 mV ($vs.$ Ag|AgCl). The Aβ-AuNP$_{ass}$@WO_3/FTO electrode shows photocurrent density of $ca.$ 54 μA cm^{-2} in the fifth irradiation, which is significantly increased relative to that found in WO_3/FTO electrode ($ca.$ 24 μA cm^{-2}) and LA-AuNP@WO_3/FTO ($ca.$ 25 μA cm^{-2}). Interestingly, the Aβ-AuNP@WO_3/FTO electrode prepared at pH 11 has considerably lower photocurrent density of $ca.$ 32 μA cm^{-2}. The results

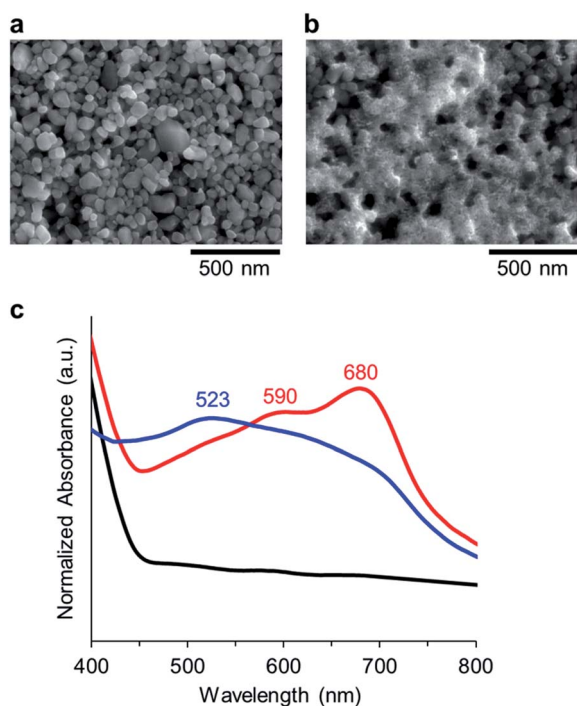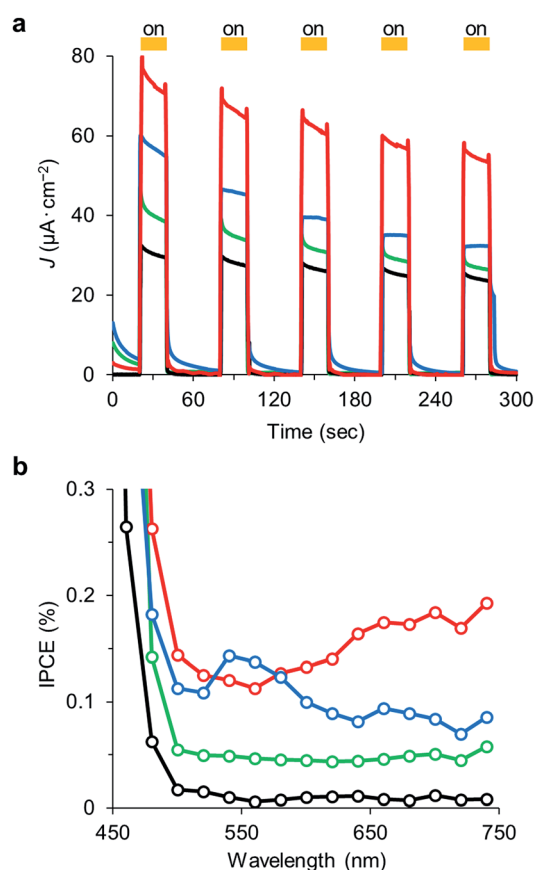**Fig. 5** (a) Photocurrent response of WO_3/FTO (black), LA-AuNP@WO_3/FTO (green), Aβ-AuNP$_{dis}$@WO_3/FTO (blue), and Aβ-AuNP$_{ass}$@WO_3/FTO (red) during on−off cycles of visible light irradiations ($λ = 420-750$ nm). Photoanodes under constant bias voltage at +300 mV ($vs.$ Ag|AgCl) in 1.0 M KOH with 0.5 M 2-propanol. The photocurrent response of Aβ-AuNP$_{ass}$@WO_3/FTO decreases to the similar level of WO_3/FTO after a 10 min irradiation. (b) Action spectra of WO_3/FTO (black), AuNP@WO_3/FTO (green), Aβ-AuNP$_{dis}$@WO_3/FTO (blue), and Aβ-AuNP$_{ass}$@WO_3/FTO (red). IPCE values are averaged through three independent experiments.

Fig. 4 SEM images of (a) WO_3/FTO, and (b) Aβ-AuNP$_{ass}$@WO_3/FTO. (c) Diffuse reflection spectra of WO_3 (black), Aβ-AuNP$_{dis}$@WO_3/FTO (blue), and Aβ-AuNP$_{ass}$@WO_3/FTO (red).

indicate that the morphology of AuNP on the WO_3 surface significantly improves the visible light response in photocurrent generation. In addition, the stability of response over the longer cycling period in Aβ-AuNP$_{ass}$@WO_3/FTO is improved relative to that in Aβ-AuNP$_{dis}$@WO_3/FTO.

The action spectrum of the Aβ-AuNP$_{ass}$@WO_3/FTO electrode exhibits a gradual increase in current efficiency above 550 nm corresponding to its absorption spectrum (Fig. 5b). In contrast, the spectrum of Aβ-AuNP$_{dis}$@WO_3/FTO has a peak at 550 nm. The WO_3/FTO and LA-AuNP@WO_3/FTO electrodes do not show peak maxima above 500 nm. The results also support the evidence that shifted SPR promotes the photocurrent generation upon the visible light irradiation.

The tight assembly of plasmonic AuNPs immobilized on the WO_3 surface would enhance light absorbance around the absorption edge.[10] In addition, clear but not intense IPCE maximum that corresponds to the plasmon absorption peak suggests the effective generation of hot electrons, leading to photocurrent increase (Fig. 6).[11]

In conclusion, we prepared an AuNP–WO_3 composite immobilizing the AuNP assembly which is connected using an Aβ peptide and investigated the photocurrent generation activity of the composites with visible light-irradiation. The AuNPs modified with Aβ peptides were confirmed to be assembled as a fibrous nanostructure, enabling the absorption of visible light at 650 nm. In addition, the Aβ-AuNP assembly fabrication on a FTO electrode is more effective than the composites such as Aβ-AuNP$_{dis}$@WO_3 or WO_3 without AuNP with respect to photocurrent generation upon visible light irradiation. The results indicate that the fibrous AuNP assembly on the WO_3 surface greatly improves SPR-assisted light absorption of the AuNP–WO_3 composite photoelectrode. This work demonstrates that fabricated noble metal nanoparticle assemblies on semiconductor materials can be precisely designed as visible light responsive photocatalysts. It is expected that further studies of such metal nanoparticle–semiconductor composites using Aβ peptides will significant insights into our understanding of the photocatalytic behavior of semiconductor nanomaterials.

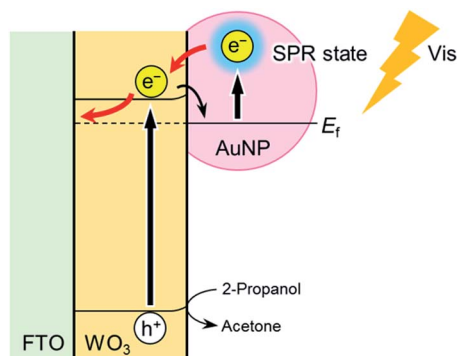Fig. 6 Schematic representation of surface plasmon-induced photocurrent generation.

Notes and references

1 N. Zhou, V. Lopez-Puente, Q. Wang, L. Polavarapu, I. Pastoriza-Santos and Q.-H. Xu, *RSC Adv.*, 2015, **5**, 29076–29097.

2 A. Primo, A. Corma and H. Garcia, *Phys. Chem. Chem. Phys.*, 2011, **13**, 886–910.

3 S. G. Kumar and L. G. Devi, *J. Phys. Chem. A*, 2011, **115**, 13211–13241.

4 P. V. Kamat, *J. Phys. Chem. Lett.*, 2012, **3**, 663–672.

5 H. Tada, T. Kiyonaga and S. I. Naya, *Chem. Soc. Rev.*, 2009, **38**, 1849–1858.

6 S. Linic, P. Christopher and D. B. Ingram, *Nat. Mater.*, 2011, **10**, 911–921.

7 J. S. DuChene, B. C. Sweeny, A. C. Johnston-Peck, D. Su, E. A. Stach and W. D. Wei, *Angew. Chem., Int. Ed.*, 2014, **53**, 7887–7891.

8 D. B. Ingram, P. Christopher, J. L. Bauer and S. Linic, *ACS Catal.*, 2011, **1**, 1441–1447.

9 D. Hu, P. Diao, D. Xu and Q. Wu, *Nano Res.*, 2016, **9**, 1735–1751.

10 R. Solarska, K. Bienkowski, S. Zoladek, A. Majcher, T. Stefaniuk, P. J. Kulesza and J. Augustynski, *Angew. Chem., Int. Ed.*, 2014, **53**, 14196–14200.

11 F. Xu, Y. Yao, D. Bai, R. Xu, J. Mei, D. Wu, Z. Gao and K. Jiang, *RSC Adv.*, 2015, **5**, 60339–60344.

12 A. Tanaka, K. Hashimoto and H. Kominami, *J. Am. Chem. Soc.*, 2013, **136**, 586–589.

13 T. He, Y. Ma, Y. Cao, W. Yang and J. Yao, *Phys. Chem. Chem. Phys.*, 2002, **4**, 1637–1639.

14 S. Zou and G. C. Schatz, *Chem. Phys. Lett.*, 2005, **403**, 62–67.

15 Z. Liu, W. Hou, P. Pavaskar, M. Aykol and S. B. Cronin, *Nano Lett.*, 2011, **11**, 1111–1116.

16 P. Spinelli, M. Hebbink, R. de Waele, L. Black, F. Lenzmann and A. Polman, *Nano Lett.*, 2011, **11**, 1760–1765.

17 H. Harada, A. Onoda, T. Uematsu, S. Kuwabata and T. Hayashi, *Langmuir*, 2016, **32**, 6459–6467.

18 J. Hardy and D. J. Selkoe, *Science*, 2002, **297**, 353–356.

19 K. Yokoyama and D. R. Welchons, *Nanotechnology*, 2007, **18**, 105101.

20 A. Majzik, L. Fülöp, E. Csapó, F. Bogár, T. Martinek, B. Penke, G. Bíró and I. Dékány, *Colloids Surf., B*, 2010, **81**, 235–241.